

Periodicity, Mixed-Mode Oscillations, and Quasiperiodicity in a Rhythm-Generating Neural Network

Christopher A. Del Negro,* Christopher G. Wilson,* Robert J. Butera,[†] Henrique Rigatto,[‡] and Jeffrey C. Smith*

*Cellular and Systems Neurobiology Section, Laboratory of Neural Control, National Institute of Neurological Disorders and Stroke, National Institutes of Health, Bethesda, MD 20892 USA, [†]Laboratory for Neuroengineering, Georgia Institute of Technology, Atlanta, GA 30332 USA, and [‡]Departments of Pediatrics and Physiology, University of Manitoba, Winnipeg, Manitoba R3T 2N2, Canada

ABSTRACT We studied patterns of oscillatory neural activity in the network that generates respiratory rhythm in mammals. When isolated *in vitro*, this network spontaneously generates an inspiratory-related motor rhythm, with stable amplitude from cycle to cycle. We show that progressively elevating neuronal excitability *in vitro* causes periodic modulation of this inspiratory rhythm, evoking (in order): mixed-mode oscillations, quasiperiodicity, and ultimately disorganized aperiodic activity. Thus, the respiratory network oscillator follows a well defined sequence of behavioral states characterized by dynamical systems theory, which includes discrete stages of periodic and quasiperiodic amplitude modulation and progresses (according to theory) to aperiodic chaos-like behavior. We also observed periodic, mixed-mode periodic, and quasiperiodic breathing patterns in neonatal rodents and human infants *in vivo*, suggesting that breathing patterns generated by the intact nervous system reflect deterministic neural activity patterns in the underlying rhythm-generating network.

INTRODUCTION

Many physical and biological systems consist of networks of coupled oscillators (Strogatz, 2001). These complex systems generate a wide variety of collective behaviors that include periodic, quasiperiodic, and aperiodic rhythms, which putatively underlie empirical phenomena such as physiological and pathophysiological oscillations (Dano et al., 1999; Glass, 2001), cardiac arrhythmia (Garfinkel et al., 1997), fluid turbulence (Ott, 1993; Ruelle and Takens, 1971), spiral waves and cluster patterns in excitable media (Petrov et al., 1997; Qu et al., 1999; Steinbock et al., 1993; Vanag et al., 2000), and deterministic chaos in many forms (Kaneko and Ichiro, 2000; Nayfeh and Balachandran, 1995; Ott, 1993).

A critical unanswered question is what dynamic patterns can emerge in networks of synaptically coupled oscillatory neurons in the brain, which may have functional consequences for neural systems that generate rhythmic patterns, including neural rhythms underlying motor behaviors such as breathing, locomotion, and mastication (Marder and Calabrese, 1996; Stein et al., 1997). We studied this issue using the mammalian respiratory oscillator as a model brain system. Critical components of this network are located in a structurally and functionally specialized region of the lower brain stem called the pre-Bötzinger complex (pre-BötC), which putatively contains key elements of the neuronal kernel generating inspiratory rhythm (Rekling and Feldman, 1998; Smith et al., 1991, 2000). *In vitro* brain stem slices

from neonatal rodents that isolate the pre-BötC spontaneously generate inspiratory-related motor activity (Koshiya and Smith, 1999; Smith et al., 1991), providing an optimal experimental system for recording and analyzing oscillatory neural activity related to respiration under conditions in which parameters affecting network behavior can be controlled.

In this study we use techniques from nonlinear dynamics and experimental electrophysiology to analyze neuron population activity over a wide range in levels of network excitability, which is a tunable parameter in the nervous system controlling rhythm generation in the respiratory network (Butera et al., 1999b; Del Negro et al., 2001). We show that the respiratory oscillator systematically progresses from stable periodic activity to disorganized aperiodic activity (with intermediate stages of periodic and quasiperiodic amplitude modulation) as neuronal excitability is elevated. This is the first such demonstration in a neural system. Also, we analyze breathing patterns in neonatal rats and human infants to determine whether similar dynamics are reflected in the system-level behavior *in vivo*, where the rhythm-generating kernel is embedded in the intact nervous system.

METHODS

Experimental methods

In vitro brain stem slice preparation

We cut 350- μm -thick transverse slices from the medulla of neonatal rats (P0-P3) with rostral and caudal ends bordering the pre-BötC in artificial cerebrospinal fluid (ACSF) containing (in mM): 128.0 NaCl, 3.0 KCl, 1.5 CaCl₂, 1.0 MgSO₄, 21.0 NaHCO₃, 0.5 NaH₂PO₄, and 30.0 D-glucose, equilibrated with 95% O₂ and 5% CO₂ (27°C, pH = 7.4), as originally described (Smith et al., 1991). Slices were fixed in a 2-ml recording chamber and perfused with ACSF at 5 ml/min. Rhythmic respiratory

Received for publication 6 July 2001 and in final form 19 September 2001.

Address reprint requests to Dr. Jeffrey C. Smith, Laboratory of Neural Control, National Institute of Neurological Disorders and Stroke, NIH, 49 Convent Drive, MSC 4455, Bethesda, MD 20892-4455; Tel.: 301-496-4960; Fax: 301-402-4836; E-mail: jsmith@helix.nih.gov.

© 2002 by the Biophysical Society

0006-3495/02/01/206/09 \$2.00

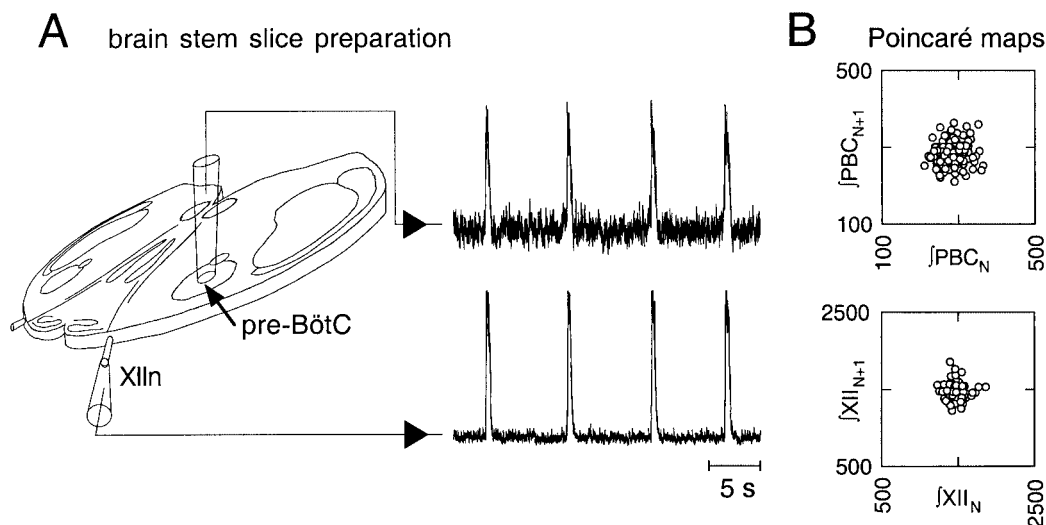


FIGURE 1 (A) 350- μm -thick brain stem slice preparation containing the pre-BötC in the ventrolateral medulla and hypoglossal nerve rootlets (XIIIn). Neural population activity recorded locally in the pre-BötC via suction electrodes is shown rectified and smoothed by analog “leaky” integration. Time calibration is shown and $[\text{K}^+]_o = 8 \text{ mM}$. (B) Examples of Poincaré maps of inspiratory burst area obtained from measurements of pre-BötC population activity and XIIIn (burst area in arbitrary V-ms units). The scale of the XIIIn Poincaré map reflects the greater signal-to-noise ratio obtained via the XIIIn suction electrodes compared with local pre-BötC recordings. Both Poincaré maps were judged to be single-point clusters by spatial statistics (see Methods).

activity was maintained by raising the ACSF K^+ concentration ($[\text{K}^+]_o$) to $\geq 8 \text{ mM}$. Inspiratory-related motor discharge (Smith et al., 1990) was recorded from the hypoglossal nerve (XIIIn) rootlets (which contains the axons for hypoglossal motoneurons also captured in the slice) with fire-polished glass suction electrodes (60–90 μm inner diameter) and a Cyber-amp (Axon Instruments, Union City, CA). Inspiratory neuron population activity was simultaneously recorded locally in the pre-BötC using “macro-patch” suction electrodes ($\sim 100 \mu\text{m}$ inner diameter) applied to the slice surface (Fig. 1 A and Del Negro et al., 2001). Population recordings were made from the caudal surface of the slice, which putatively exposes rhythm-generating neurons (Koshiya and Smith, 1999). The XIIIn and pre-BötC recordings were rectified and smoothed by analog “leaky” integration (50-ms time constant), which enhanced the signal-to-noise ratio and thus improved our ability to analyze data quantitatively.

Measurements of breathing patterns in vivo

We recorded spontaneous breathing patterns in intact neonatal rats (P0-P4) in vivo using a noninvasive, nonsurgical head-out plethysmograph, which isolates the thorax and limbs in a custom-made sealed chamber coupled to a pressure transducer (Micron Instruments MP-15, Simi Valley, CA). Inspired tidal volume (VT) was calculated from pressure changes, which were calibrated by 200- μl room-air injections from a syringe. Animals were tested in two conditions: the awake, behaving state and after light urethane anesthesia (0.5 mg/kg, Sigma Chemical, St. Louis, MO). Breathing patterns were qualitatively identical in both conditions. Light anesthesia only reduced the number of movement artifacts during plethysmography and thus allowed longer duration stationary recordings, which improved breathing-pattern analysis by adding more points from consecutive breaths to the Poincaré maps (see below). In some animals we used diaphragmatic electromyography (EMG) to record inspiratory activity. These animals were deeply anesthetized with urethane (1.5 mg/kg) until they failed to respond to tail-pinch tests. Silver Teflon-coated (DuPont, Wilmington, DE) fine-gauge wires were inserted into the diaphragm near the costal margin and electrical activity monitored via high-impedance probes (Axon Instruments). All animals were maintained at physiological temperature (37°C). All animal procedures were approved by the institu-

tional Animal Care and Use Committee and adhered to National Institutes of Health guidelines.

Breathing patterns of human infants in a resting state were recorded using a noninvasive pneumotachygraph coupled to a pressure transducer, providing signals proportional to airflow that were digitally integrated to obtain VT. These recordings were performed under the supervision and care of a pediatrician (H.R.) in nine infants of the following ages (in days): 6, 6, 7, 14, 19, 26, 35, 46, and 71. No age-specific differences were observed between 6–71 days, so these data were analyzed as a single infant sample population. Parental consent was given and procedures conformed to institutional guidelines (Women’s Hospital, University of Manitoba).

Signal acquisition and analysis

Neurophysiological, EMG, and plethysmographic signals were low-pass filtered at 1 kHz and acquired digitally at 4 kHz to prevent “aliasing.” Digital acquisition and analysis used Chart software and PowerLab (AD Instruments, Mountain View, CA). We measured inspiratory burst amplitude and computed the burst area from rectified and smoothed signals using automated algorithms hand-checked for accuracy. Burst area and amplitude were tightly correlated and thus analyzed interchangeably. In general, burst area measurement was more robust than amplitude measurement at lower signal-to-noise ratios and thus was our preferred measure in most experiments.

Poincaré maps and spatial statistics

We constructed Poincaré maps (also known as next-amplitude return maps, as described in Results and in Nayfeh and Balachandran, 1995) from the area or amplitude of inspiratory bursts. Let x represent measurement of either burst area or amplitude. Poincaré return maps plot the $n + 1$ th observation (x_{n+1}) versus the n th observation (x_n) for a sequence of observations $n = 0, 1, 2, \dots, m-1$ (where m is the number of bursts in sequence measured during a stationary recording epoch). The map contains the same x values on both axes, but a distinct geometric form emerges if the observations occur in a deterministic sequence, that is $x_{n+1} = F(x_n)$ for

map F , which samples the full dynamical system. The geometric form can be used to diagnose the underlying dynamics (Abraham and Shaw, 1992), which we demonstrate in Results. We used spatial (Ripley, 1981) and scalar statistics (Snedecor and Cochran, 1989) to quantitatively judge the geometric form of Poincaré maps. For example, the Poincaré map of a simple periodic system contains one point (Fig. 4 and Results). In a corresponding biological system with noise, this single point becomes a normally distributed single-point cluster. The form of our Poincaré map was considered to be a normally distributed single-point cluster if the datapoints along one axis were (1) unimodal without significant skew and (2) passed a χ^2 test for normality.

If a rhythmic system is periodically modulated and its output alternates between discrete amplitudes, then it can be considered a “mixed-mode oscillation.” This type of system produces several distinct points in the Poincaré map (Fig. 4 and Results). In biological systems with noise, the points become multiple, normally distributed point clusters. Therefore, if a Poincaré map failed the above test for a single-point cluster, then we next considered whether the map contained multiple point clusters. Multiple clusters were indicated if the point distribution along one axis was (1) bimodal with significant skew, (2) failed the χ^2 test for normality, and (3) also failed the test for “ring” structure.

In advanced stages of periodic modulation, the fundamental rhythm and its modulation can have incommensurate frequencies (i.e., their ratio is an irrational number). In this case the system is “quasiperiodic” and is evaluated by ring-like structures in the Poincaré map (see Results and Fig. 4 C for cross-section of a quasiperiodic system). To classify a ring-like Poincaré map, we identified the central hole that exists in ring-structures according to the test by Garfinkel et al. (1997): if a hole exists, then few points are located at short radial distances from its center. We computed this radial distance r for each datapoint by selecting a center within the ring and transforming from Euclidean to polar coordinates ($r = \sqrt{x^2 + y^2}$, $\theta = \arctan(x/y)$), then sorting the distances in a 20-bin histogram for radii. We then randomized (shuffled) the sequence of observations, which eliminates the empirical relationship between x_n and x_{n+1} , reconstructed the Poincaré map from the surrogate data, and computed a new histogram of radial distances. After 100 shuffles, if the tally for the smallest-radius bin contained fewer counts than any of the 100 histograms compiled from surrogate data, then a statistically significant hole exists in the original data at $P < 0.01$.

If a sequence of inspiratory bursts produced a Poincaré map that (1) failed the χ^2 test for normality, (2) was unimodal with significant skew, and (3) failed the test for rings, then the system behavior was considered aperiodic because its Poincaré map was formless. In this case we could not evaluate network dynamics from the map.

RESULTS

We analyzed network dynamics at the neuron-population level in the pre-BötC in vitro using Poincaré maps of inspiratory burst area, which successively plot the present measure of pre-BötC activity ($\int\text{PBC}_{n+1}$) versus its previous value ($\int\text{PBC}_n$) for a continuous sequence of inspiratory bursts (Fig. 1). If network behavior is deterministic then the present state is determined by previous states and the Poincaré map exhibits a distinct geometric form (Abraham and Shaw, 1992; Nayfeh and Balachandran, 1995). According to embedding theory, the Poincaré map is topologically equivalent to a Poincaré surface of section that intersects the system's trajectory in its characteristic state-space (Sauer et al., 1991). Therefore, the geometric form of the Poincaré map can be used to identify an underlying attractor, a stable trajectory for a system that “attracts” all initial states within

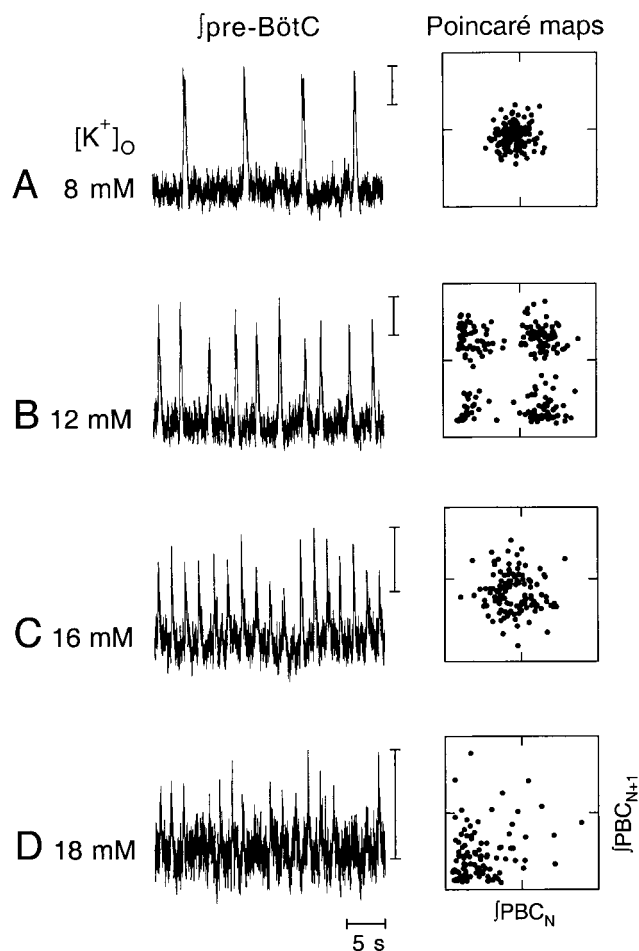


FIGURE 2 The dynamics of inspiratory rhythms recorded in vitro. (A–D) Rhythms in the pre-BötC at ascending $[\text{K}^+]_o$ (8–18 mM) and corresponding Poincaré maps of inspiratory burst area. Vertical calibration bars show 1 V for each trace (after amplification by 50,000). The ordinate axes for time series and Poincaré maps were expanded to maximize display, which is necessary, as inspiratory burst magnitude declines monotonically with increasing $[\text{K}^+]_o$ (Del Negro et al., 2001). Area in $\int\text{pre-BötC}$ Poincaré maps is in arbitrary units (not displayed); abscissa and ordinate have the same range.

a given region (its “basin”) and represents the final characteristic behavior of the system for those sets of initial conditions, if such an attractor exists.

In general, pre-BötC activity is accurately reflected by XII motor discharge (Del Negro et al., 2001) and Poincaré maps from $\int\text{pre-BötC}$ and $\int\text{XII}$ contained the same geometric patterns (compare Fig. 1 B, top and bottom). Nevertheless, because we were specifically interested in pre-BötC network dynamics, we always analyzed Poincaré maps created from direct measurements of pre-BötC population activity (Fig. 1 B, top). Under standard conditions in vitro (Figs. 1 B and 2 A), the Poincaré map formed a single-point cluster (as verified by spatial statistics, see Methods), which shows that the inspiratory burst had the same area (ampli-

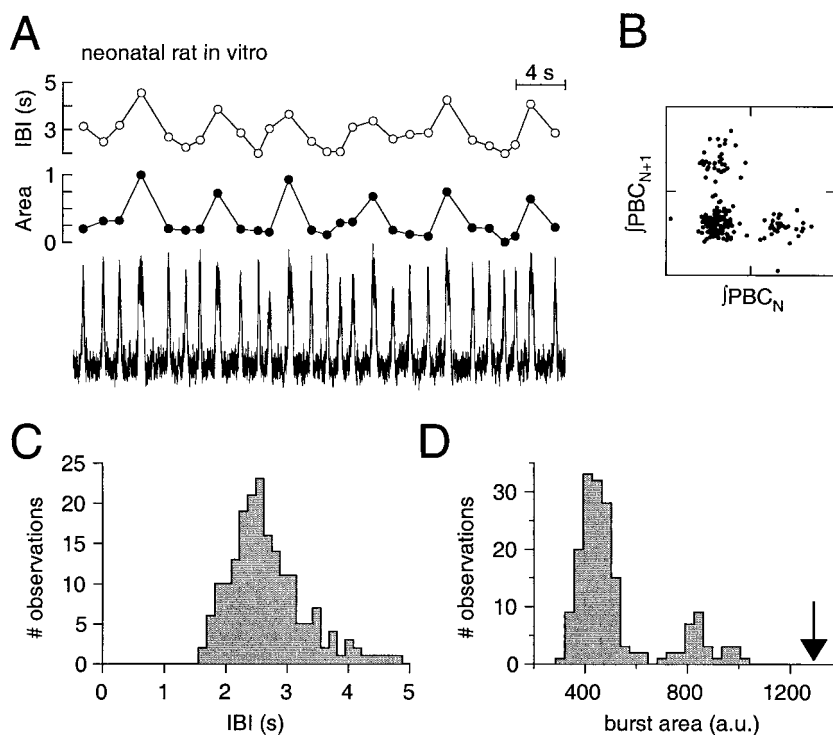


FIGURE 3 Mixed-mode oscillations in vitro. (A) Inspiratory mixed-mode oscillations in a slice preparation at 12 mM $[K^+]_o$. The area of inspiratory bursts is plotted above the time series in arbitrary normalized units with the IBIs in seconds. The IBI plotted above each burst corresponds to the interval between the present and next burst in the series. (B) Poincaré map from data in A. (C) IBI histogram from data in part A. (D) Inspiratory burst area distribution; arrow shows the sum of mean peaks at 450 and 810 arbitrary area units (a.u.).

tude) from cycle to cycle. This stable and repeating pattern is created by a system that flows toward a closed-loop path called a limit-cycle attractor and intersects its Poincaré surface of section at one characteristic point (Fig. 4 A).

Periodic modulation of inspiratory rhythms

Breathing frequency in vivo varies by an order of magnitude depending on physiological conditions. The neural basis for frequency control putatively includes modulation of neuronal excitability in the pre-BötC (Butera et al., 1999b; Gray et al., 1999; Smith et al., 2000). Therefore, we examined how changes in cell excitability affected network dynamics in vitro. A typical experiment is shown in Fig. 2. We controlled excitability by varying K^+ concentration ($[K^+]_o$) in the bathing solution, which affects the electrochemical gradient for K^+ currents that set baseline membrane potential in respiratory neurons. Fig. 2 A shows periodic network activity at basal excitability (i.e., a limit cycle at 8-mM $[K^+]_o$). Fig. 2 B shows network activity after raising $[K^+]_o$ to 12 mM. Elevating the excitability increased inspiratory frequency and caused burst amplitude fluctuations between two discrete levels, which produced several distinct point clusters in the Poincaré map.

Similar data obtained at 12-mM $[K^+]_o$ in a different slice preparation are shown in Fig. 3 A. In this case, low-frequency periodic modulation takes the form of augmented inspiratory bursts that recur rhythmically (area measurements are plotted above the time series), and which form three point clusters in the Poincaré map. The behavior in Figs. 2 B and 3 A resembles a mixed-mode oscillation, which occurs if a rhythmic system possesses two or more characteristic periods, and the ratio of the periods is an integer.

For example, if a system contains two rhythmic processes with periods P_N and P_M , where N is the fundamental rhythm and M is its modulation and the ratio $P_M/P_N = 4$, then the system-level output ($N + M$) will be augmented by M during every fourth N cycle. The output of the system will alternate between two levels such that one full cycle is described by this repeating sequence: $N, N, N, N + M$. Thus, in mixed-mode oscillations, burst amplitude is periodically modulated but returns to the same set of discrete values repeatedly (Fig. 4 B for illustration and Nayfeh and Balachandran, 1995, for more a comprehensive treatment of mixed-mode oscillations).

If the discrete amplitude fluctuations we observed in the pre-BötC data (Figs. 2 B and 3, A and B) do not result from

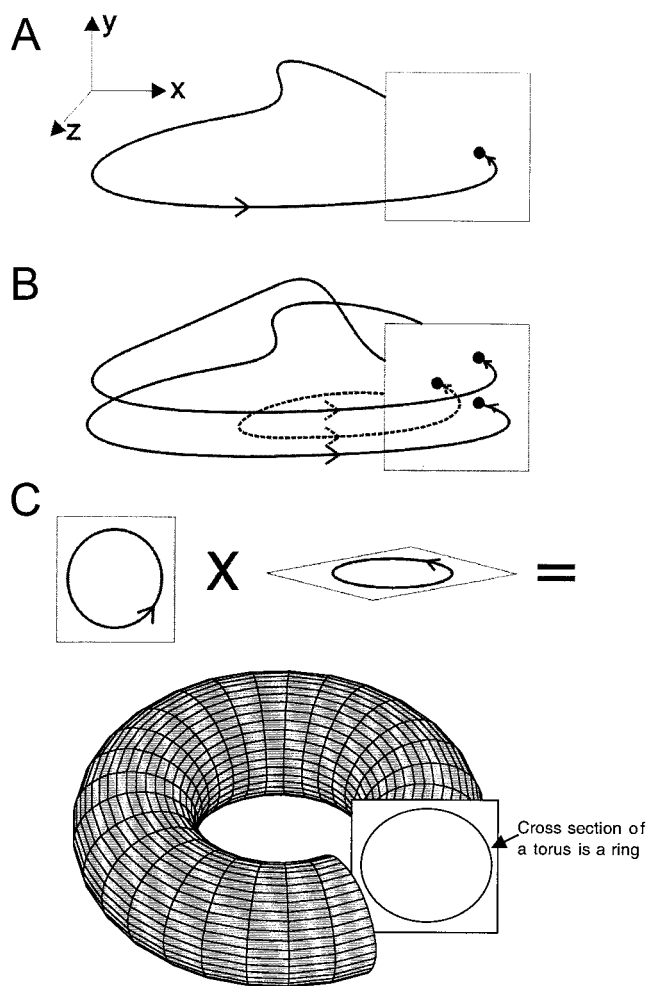


FIGURE 4 State-space behaviors and Poincaré sections. (A and B) Three-dimensional state space is illustrated. (A) A limit-cycle with one period and its characteristic Poincaré section (map) with a single point. (B) A mixed-mode oscillation and multiple points in its Poincaré section (map). (C) Toroidal state space resulting from the product of two cyclic variables; a quasiperiodic system flows on the toroidal surface. The upper portion illustrates two separate periodic processes with incommensurate periods, which when coupled together, give rise to the torus shown in the lower portion. The torus is severed to show that its cross-section, or Poincaré section, is a ring. These cartoons illustrate how distinct geometric patterns formed in the Poincaré maps (topologically equivalent to Poincaré sections) are obtained from the trajectories of each system.

a mixed-mode oscillation, then the amplitude fluctuations must reflect uncoupled independent periodic processes that are incidentally recorded by the same macropatch electrode in vitro. If this were the case, then two specific predictions arise. First, the large and small amplitude bursts would not be temporally correlated because both processes would be independent and free-running. Therefore, the distribution of interburst intervals (IBIs) would be negatively skewed and would contain intervals ranging from a minimum of 0^+ , reflecting two nearly synchronous independent bursts, to a maximum interval equal to the period (\pm SD) of the fun-

damental inspiratory rhythm. In this scenario, the maximum IBI is equal to the period of the faster periodic process, which is the inspiratory rhythm because it is by definition faster than its periodic modulation. Two inspiratory bursts may occur in sequence without an intervening larger burst (which has a lower intrinsic frequency) in the same time window. In all other cases, according to this scenario, inspiratory bursts are separated by an intervening augmented burst and the period must therefore be less than the period of the inspiratory cycle that gets interrupted. In regard to the second prediction, if two independent and free-running processes have discrete burst amplitudes, then eventually the large and small bursts will occur synchronously, producing a third burst with amplitude equal to the sum of the other two. In no slice preparations were either of these two predictions confirmed ($n = 20$ slices at 3 or more different $[K^+]_o$ levels all recorded for ≥ 20 min). Fig. 3 C shows the IBI distribution for the data in part A. This distribution is not negatively skewed and there were no IBIs near to 0^+ s (in fact, no IBIs < 1.5 s were observed). Instead, the IBI distribution is positively skewed because the augmented bursts slightly delay the subsequent lower amplitude inspiratory bursts. Fig. 3 A (top row) shows the IBI plotted above each burst in series; note that augmented bursts are followed by long duration IBIs. This effect has previously been shown in the pre-BötC of neonatal mice (Lieske et al., 2000). The subsequent delay induced by augmented bursts creates a subset of long duration IBIs that positively skews the IBI distribution (Fig. 3 C), and suggests that the large and small amplitude bursts interact. Regarding the second prediction, Fig. 3 D shows the burst amplitude histogram is bimodal with two (not three) inspiratory burst amplitudes; an arrow shows the sum of the two means (for burst area) with zero observations. These data suggest that the amplitude fluctuations in vitro do not reflect uncoupled and independent free-running periodic processes. The data are more consistent with a mixed-mode oscillation in the pre-BötC network, in which two (or more) periodic processes interact resulting in deterministic periodic modulation of the inspiratory rhythm.

At $[K^+]_o > 12$ mM, the inspiratory burst amplitude varied continuously, instead of discretely, suggesting a qualitative change in the periodic modulation of inspiratory activity. If the inspiratory cycle and its modulation have incommensurate periods then the system is quasiperiodic. A quasiperiodic system with two periods evolves on the surface of a doughnut-shaped 2-torus. In this case, the state space (the torus) is composed of two cyclic variables: the inspiratory rhythm and its periodic modulation. Because the two periods are not related by an integer but are incommensurate, the system does not flow toward a closed path but instead orbits without converging on the surface of the torus. Therefore, successive intersections with a Poincaré section process around a ring-like structure (Fig. 4 C and Nayfeh and Balachandran, 1995). Fig. 2 C shows ring-like

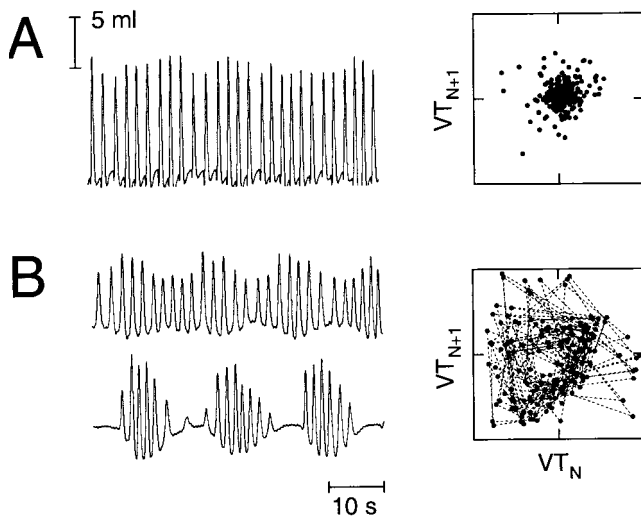


FIGURE 5 Time series of VT in human infants and associated Poincaré maps of VT. (A) A stable limit cycle breathing pattern. (B) Quasiperiodic breathing patterns, upper and lower traces from the same baby. Time and volume calibrations shown apply to all traces. Points in the Poincaré map are connected with broken lines to emphasize the central “hole” in the ring.

structures in the Poincaré map of pre-BötC neural population activity, which we typically observed at 14–16 mM $[K^+]_o$ (in $n = 17$ of 20 slices tested). Ring geometry in the Poincaré maps were distinguished from single and multiple point cluster patterns using spatial statistics (see Methods and Garfinkel et al., 1997; Ripley, 1981).

At $[K^+]_o > 16$ mM inspiratory bursts fluctuated aperiodically, creating formless Poincaré maps ($n = 10$ of 10 slices tested at $[K^+]_o > 16$ mM) that could reflect high-dimensional spatiotemporal chaos or uncoordinated phasic spiking in cells of the network (Fig. 2 D). We could not determine whether chaos was present using analytic methods (e.g., calculation of Lyapunov exponents or fractal dimension) because the inherent noise of electrophysiological recordings in a slice preparation prevented accurate orbit reconstruction using the method of time delays (Nayfeh and Balachandran, 1995; Packard et al., 1980).

Breathing patterns recorded in vivo

Lesions of the pre-BötC in vivo abolish normal respiratory movements in awake, behaving rats (Gray et al., 2001), which is consistent with the hypothesis that normal breathing movements originate in pre-BötC networks. To test whether rhythmic patterns recorded in the pre-BötC in vitro might also be observed during spontaneous breathing in vivo, we monitored respiratory movements in 15 neonatal rats and nine human infants. Fig. 5 A shows VT for stable ventilation in a human infant; this was the only infant we observed with limit-cycle dynamics. Fig. 5 B shows quasiperiodic breathing in a different infant, indicated by periodic

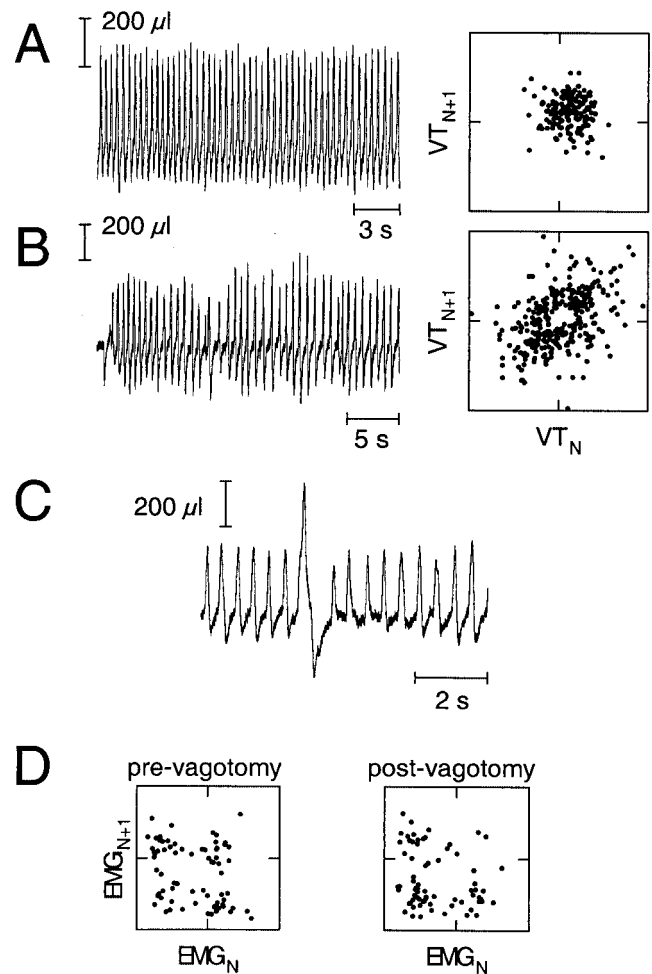


FIGURE 6 Time series of VT in neonatal rats and associated Poincaré maps of VT. (A) Stable limit cycle breathing pattern. (B) A quasiperiodic breathing pattern. Time and volume calibrations are shown. (C) An expanded trace showing an augmented inspiratory effort resembling a mixed-mode oscillation, with time and volume calibrations. (D) Quasiperiodic inspiratory patterns measured by diaphragmatic EMG before and after vagotomy in the same neonatal rat. Poincaré maps of EMG amplitude are shown; both show statistical significance for ring shapes at $P < 0.05$.

modulation in the time series and confirmed by ring-structure in the Poincaré map. This infant sometimes exhibited stationary quasiperiodic breathing with short apneic intervals (compare upper and lower time-series traces in Fig. 5 B). We recorded quasiperiodic breathing patterns in a total of four infants. Three infants exhibited recurring augmented large-amplitude inspiratory efforts resembling a mixed-mode-like oscillation (not shown). This pattern was typically not stationary enough in the available data to construct Poincaré maps with sufficiently high density of points. In neonatal rats we observed stable (limit cycle) breathing in two rat pups (Fig. 6 A) and epochs of quasiperiodic breathing in five pups (Fig. 6 B). Mixed-mode-like breathing patterns with very low frequency augmented inspiratory movements were recorded in eight rat pups (Fig. 6 C).

In the whole animal the pre-BötC is embedded in an extensive brain system that incorporates mechanosensory feedback, which could produce rhythmic instabilities. To test whether periodic modulation of breathing required sensorimotor feedback, we recorded diaphragmatic EMG in eight deeply anesthetized neonatal rats before and after severing afferent sensory feedback conveyed by the vagus nerve. Before vagotomy, 2 rat pups showed rhythmic augmented inspiratory discharges resembling mixed-mode oscillations, 4 pups showed quasiperiodic breathing, and 2 pups showed aperiodic patterns with formless Poincaré maps. After vagotomy, 1 pup showed mixed-mode oscillation, 4 pups showed quasiperiodic breathing, and 3 pups were aperiodic. Thus, vagotomy did not abolish periodic modulation and quasiperiodic breathing as shown in Fig. 6 *D* (same animal before and after vagotomy) by persistent ring-like structures in the Poincaré map. Similar ring-like Poincaré maps were obtained before and after vagotomy in two pups. Poincaré maps with multiple clusters were observed before and after vagotomy in one pup. In the other neonatal rats vagotomy had no consistent effect: inspiratory dynamics and Poincaré maps either progressed from mixed-mode oscillations or quasiperiodicity to aperiodicity ($n = 3$), or regressed from aperiodicity to quasiperiodicity ($n = 2$). These data suggest that periodic modulation of breathing patterns was not primarily attributable to sensory feedback, and could instead directly result from brain stem respiratory networks that incorporate the pre-BötC.

DISCUSSION

We have shown that increasing neuronal excitability in the respiratory network contained in the pre-BötC *in vitro* causes periodic modulation of the inspiratory rhythm. The system proceeds from periodicity to mixed-mode oscillations, quasiperiodicity, and ultimately disorganized aperiodic activity. This sequence suggests the “quasiperiodic transition to chaos” identified in a variety of rhythmic dynamical systems (Nayfeh and Balachandran, 1995; Newhouse et al., 1978; Ruelle and Takens, 1971) and now identified for the first time in a rhythm-generating neural network. We showed similar (although not identical) breathing dynamics in neonatal rats and human infants *in vivo*. Our results suggest that the respiratory network oscillator exhibits dynamics at the network-population level that periodically modulates and can destabilize the fundamental inspiratory rhythm, which may influence breathing movements *in vivo*.

Principles of network operation and neurophysiological mechanisms

The dynamic behavior of any network depends on the properties of its nodes and the geometry and nature of

coupling between nodes (Strogatz, 2001). In the nervous system the nodes (neurons) are dynamical systems: nonlinear excitable oscillators with several degrees of freedom broadly tuned by cellular excitability parameters. Also, the coupling between nodes has many degrees of freedom, including one-way chemical synaptic transmission that can be excitatory or inhibitory, with large amplitude and rapid kinetics (ionotropic receptors) or small amplitude and slow kinetics (metabotropic receptors), or alternatively two-way electrotonic coupling mediated by gap junctions between neighboring cells. Synaptic connections can also have different strengths depending on their morphological location.

The possible emergent behaviors in a network with the aforementioned properties seem virtually unlimited. In model networks designed to mimic the nervous system such as a set of identical autonomous oscillators coupled with a variety of geometric schemes (Strogatz, 2001), or lattices of logistic-map dynamical systems (May, 1976) for nodes and idealized coupling patterns (Kaneko and Ichiro, 2000), the behavioral repertoire spans many spatiotemporal patterns and routes to chaos.

Our approach to investigate what behaviors actually emerge in a mammalian rhythm-generating network has been to make accurate measurements from the network as a whole (i.e., direct recording of pre-BötC population activity) and treat it as a generic dynamical system with one observable quantity. Therefore, Poincaré maps are essential to evaluate underlying dynamics. To control cellular excitability we used a convenient and readily reversible perturbation, elevation of $[K^+]_o$, which affects baseline membrane potential and inspiratory burst frequency of constituent cells of the network (Del Negro et al., 2001). We found a subset of the patterns that can be generated in the idealized model networks alluded to above: namely, that the inspiratory rhythm was robust and periodic under standard *in vitro* conditions, and that periodic modulation resulting in mixed-mode oscillations, quasiperiodicity, and aperiodic dynamics occurred when cellular excitability was elevated.

What could give rise to periodic modulation? The rhythm-generating network in the pre-BötC contains inspiratory voltage-dependent, bursting “pacemaker” neurons that are synchronized during the inspiratory phase via fast excitatory synapses (Koshiya and Smith, 1999; Smith et al., 1991). However, pacemaker cells are autonomous bursting oscillators also capable of generating “ectopic” bursts during the interval between inspiratory phases (Butera et al., 1999a, b). Ectopic bursts are favored at higher levels of excitability and can become synchronized in subsets of cells (Del Negro et al., 2001); this may produce competing periodic rhythms at high $[K^+]_o$ that modulate the fundamental inspiratory cycle. Preliminary simulations with a heterogeneous pacemaker-network model (Butera et al., 1999b) have shown that mixed-mode and quasiperiodic rhythms can emerge via this scenario (Butera et al. 1999b; R.J. Butera and C.A. Del Negro, unpublished data).

Periodic modulation resulting in mixed-mode oscillations and quasiperiodicity have been observed in biological tissues that resemble reaction-diffusion systems because of two-way electrotonic coupling between neighboring cells, such as cardiac myocardium and pancreatic β -cell networks (de Vries, 1998; Garfinkel et al., 1997; Sherman, 1994), and in reaction-diffusion systems such as the Belousov-Zhabotinsky chemical oscillator fixed in a gel network (Steinbock et al., 1993; Vanag et al., 2000). Neural networks are not generally considered similar to reaction-diffusion systems because coupling between neurons is geometrically unconstrained; connections can occur at great distances from cell bodies via axonal and dendritic projections not based on diffusion and mediated by chemical synapses with independent kinetics. Interestingly, a recent report demonstrated electrotonic gap junction synapses between a few putatively rhythmogenic pre-BötC neurons that preferentially transmit low-frequency signals among inspiratory cells (Rekling et al., 2000). Local electrotonic coupling in arrays of inspiratory neurons (containing at least a subset of bursting pacemaker cells) may help explain the origin of low-frequency periodic modulation by facilitating the diffusion and propagation of depolarizing waves in the network. In support of this idea, a related mechanism causes spiral waves and spiral-wave meander as depolarizing waves propagate via gap junctions in the myocardium, which causes periodic modulation and quasiperiodicity in the mammalian heart (Garfinkel et al., 1997). The number and extent of gap junction synapses relative to the excitatory chemical synapses in the pre-BötC network is, however, currently unknown.

Functional implications

We have shown stable periodic, mixed-mode, and quasiperiodic breathing patterns in vivo. In vitro we found that periodic modulation in the form of mixed-mode oscillations and quasiperiodicity were inherent properties of the rhythm-generating network in the pre-BötC, and were controlled by changes in neuronal excitability. For the in vivo respiratory measurements, technically we could not systematically vary the excitability of the system to establish if the intact system trajectory proceeds from periodicity to mixed-mode oscillations, quasiperiodicity, and ultimately disorganized aperiodic activity as in vitro. Nevertheless, we observed spontaneous breathing epochs where the intact system exhibited these different dynamic states. Thus, the respiratory pattern dynamics observed in the whole animal may reflect the state of excitability of inspiratory neurons of the pre-BötC involved in rhythm-generation in the intact nervous system. As a result, changes in the level of excitability in these cells could functionally result in inadequate respiratory movements for proper ventilation under some circumstances, but this remains to be demonstrated.

This research was supported by National Institute of Neurological Disorders and Stroke (NINDS) intramural research funds and Canadian Institutes for Health Research, grant 15392. Dr. Del Negro was supported by an NINDS Intramural Competitive Fellowship Award. We thank Dr. N. Koshiya for critiques of the manuscript.

REFERENCES

- Abraham, R. H., and C. D. Shaw. 1992. Dynamics. The Geometry of Behavior. R.L. Devaney, editor. Addison-Wesley, Redwood City, CA.
- Butera, R. J. Jr., J. Rinzel, and J. C. Smith. 1999a. Models of respiratory rhythm generation in the pre-Bötzing complex. I. Bursting pacemaker neurons. *J. Neurophysiol.* 82:382–397.
- Butera, R. J. Jr., J. Rinzel, and J. C. Smith. 1999b. Models of respiratory rhythm generation in the pre-Bötzing complex. II. Populations of coupled pacemaker neurons. *J. Neurophysiol.* 82:398–415.
- Dano, S., P. G. Sorensen, and F. Hynne. 1999. Sustained oscillations in living cells. *Nature.* 402:320–322.
- de Vries, G. 1998. Diffusively coupled bursters: effects of cell heterogeneity. *Bull. Math. Biol.* 60:1167–1200.
- Del Negro, C. A., S. M. Johnson, R. J. Butera, and J. C. Smith. 2001. Models of respiratory rhythm generation in the pre-Bötzing complex. III. Experimental tests of model predictions. *J. Neurophysiol.* 86:59–74.
- Garfinkel, A., P. S. Chen, D. O. Walter, H. S. Karagueuzian, B. Kogan, S. J. Evans, M. Karpoukhin, C. Hwang, T. Uchida, M. Gotoh, O. Nwasokwa, P. Sager, and J. N. Weiss. 1997. Quasiperiodicity and chaos in cardiac fibrillation. *J. Clin. Invest.* 99:305–314.
- Glass, L. 2001. Synchronization and rhythmic processes in physiology. *Nature.* 410:277–284.
- Gray, P. A., W. A. Janczewski, N. Mellen, D. R. McCrimmon, and J. L. Feldman. 2001. Normal breathing requires preBötzing complex neurokinin-1 receptor-expressing neurons. *Nat. Neurosci.* 4:927–930.
- Gray, P. A., J. C. Rekling, C. M. Bocchiaro, and J. L. Feldman. 1999. Modulation of respiratory frequency by peptidergic input to rhythmogenic neurons in the preBötzing complex. *Science.* 286:1566–1568.
- Kaneko, K., and T. Ichiro. 2000. Complex Systems: Chaos and Beyond. Springer-Verlag, New York.
- Koshiya, N., and J. C. Smith. 1999. Neuronal pacemaker for breathing visualized in vitro. *Nature.* 400:360–363.
- Lieske, S. P., M. Thoby-Brisson, P. Telgkamp, and J. M. Ramirez. 2000. Reconfiguration of the neural network controlling multiple breathing patterns: eupnea, sighs and gasps. *Nat. Neurosci.* 3:600–607.
- Marder, E., and R. L. Calabrese. 1996. Principles of rhythmic motor pattern generation. *Physiol. Rev.* 76:687–717.
- May, R. M. 1976. Simple mathematical models with very complicated dynamics. *Nature.* 261:459–467.
- Nayfeh, A. H., and B. Balachandran. 1995. Applied Nonlinear Dynamics: Analytical, Computational, and Experimental Methods. Wiley, New York.
- Newhouse, S., D. Ruelle, and F. Takens. 1978. Occurrence of strange axiom A attractors near quasiperiodic flows on T^m , $m \geq 3$. *Commun. Math. Phys.* 64:35–40.
- Ott, E. 1993. Chaos in Dynamical Systems. Cambridge University Press, Cambridge.
- Packard, N. H., J. P. Crutchfield, J. D. Farmer, and R. S. Shaw. 1980. Geometry from a time series. *Phys. Rev. Lett.* 45:712–716.
- Petrov, V., Q. Ouyang, and H. Swinney. 1997. Resonant pattern formation in a chemical system. *Nature.* 388:655–657.
- Qu, Z., F. Xie, and A. Garfinkel. 1999. Diffusion-induced vortex instability in 3-dimensional excitable media. *Phys. Rev. Lett.* 83:2668–2671.
- Rekling, J. C., and J. L. Feldman. 1998. PreBötzing complex and pacemaker neurons: hypothesized site and kernel for respiratory rhythm generation. *Ann. Rev. Physiol.* 60:385–405.
- Rekling, J. C., X. M. Shao, and J. L. Feldman. 2000. Electrical coupling and excitatory synaptic transmission between rhythmogenic respiratory neurons in the PreBötzing complex. *J. Neurosci.* 20:RC113.
- Ripley, B. D. 1981. Spatial Statistics. Wiley, New York.

- Ruelle, D., and F. Takens. 1971. On the nature of turbulence. *Commun. Math. Phys.* 20:167–192.
- Sauer, T., J. Yorke, and M. Casdagli. 1991. Embedology. *J. Stat. Phys.* 65:579–616.
- Sherman, A. 1994. Anti-phase, asymmetric and aperiodic oscillations in excitable cells—I. Coupled bursters. *Bull. Math. Biol.* 56:811–835.
- Smith, J. C., R. J. Butera, N. Koshiya, C. A. Del Negro, C. G. Wilson, and S. M. Johnson. 2000. Respiratory rhythm generation in neonatal and adult mammals: the hybrid pacemaker-network model. *Respir. Physiol.* 122:131–147.
- Smith, J. C., H. H. Ellenberger, K. Ballanyi, D. W. Richter, and J. L. Feldman. 1991. Pre-Bötzinger complex: a brain stem region that may generate respiratory rhythm in mammals. *Science.* 254:726–729.
- Smith, J. C., J. J. Greer, G. S. Liu, and J. L. Feldman. 1990. Neural mechanisms generating respiratory pattern in mammalian brain stem-spinal cord in vitro. I. Spatiotemporal patterns of motor and medullary neuron activity. *J. Neurophysiol.* 64:1149–1169.
- Snedecor, G., and W. Cochran. 1989. *Statistical Methods*, 8th ed. Iowa State University Press, Ames.
- Stein, P., S. Grillner, A. Selverston, and D. Stuart. 1997. *Neurons, Networks, and Motor Behavior*. MIT Press, Cambridge.
- Steinbock, O., V. Zykov, and S. C. Müller. 1993. Control of spiral-wave dynamics in active media by periodic modulation of excitability. *Nature.* 366:322–324.
- Strogatz, S. H. 2001. Exploring complex networks. *Nature.* 410:268–276.
- Vanag, V. K., L. Yang, M. Dolnik, A. M. Zhabotinsky, and I. R. Epstein. 2000. Oscillatory cluster patterns in a homogeneous chemical system with global feedback. *Nature.* 406:389–391.